ELSEVIER

Materials Science and Engineering A342 (2003) 11–22

MATERIALS SCIENCE & ENGINEERING A

www.elsevier.com/locate/msea

Numerical modelling of crack shielding and deflection in a multi-layered material system

M.R. Joyce [a,*], P.A.S. Reed [a], S. Syngellakis [b]

[a] *Materials Research Group, School of Engineering Sciences, University of Southampton, Highfield, Southampton SO17 1BJ, UK*
[b] *Computational Engineering and Design Group, School of Engineering Sciences, University of Southampton, Highfield, Southampton SO17 1BJ, UK*

Received 19 November 2001; received in revised form 11 March 2002

Abstract

Finite element analysis has been used to investigate the fatigue behaviour observed in testing a layered structure (representative of an automotive journal bearing). The aim of the analysis was to explain the deflection or bifurcation observed as a fatigue crack propagates through the multi-layered structure of a bearing. A fracture mechanics approach was adopted using detailed evaluations of the J-integral to assess and monitor both crack tip driving force and directional propensity with crack growth. Crack shielding or anti-shielding as well as deflection or bifurcation were conclusively linked to the difference between the fundamental elasto-plastic properties of the various constituent materials.

Keywords: Multi-layer materials; Plain bearings; Fatigue; Crack shielding; Crack deflection

1. Introduction

Half shell bearings used in automotive main bearing and rod bearing applications operate in a complex environment placing many demands on the bearing system. Strength is required for load bearing and resistance to fatigue damage, whilst at the same time the bearing material requires 'soft properties' which impart conformability to the system and allow embedment of debris. The bearing is also required to be resistant to scuffing and seizure to the crankshaft if the hydrodynamic oil film were to become disrupted. This combination of properties is currently achieved using multi-layer material structures. These are categorised into two groups: (1) tri-metal bearings comprising three layers; a steel backing, a layer of leaded bronze and a thin soft overlay; (2) bimetal bearings comprising also three layers; a steel backing bonded to a layer of aluminium bearing material by a thin pure aluminium layer. Under normal operating conditions in an engine, fatigue failure is not normally observed, as the bearing size, type and material are selected on various design load criteria. However, the ongoing material and product development process uses extensive rig and engine testing, some of which test the bearing shells to the point of failure. Understanding the damage mechanisms is key to the development process and whilst the development of bearing materials has, over many years, been carried out in a semi-empirical manner, this paper describes how a more analytical approach is being taken to characterising their fundamental fatigue behaviour. The focus here is on the behaviour of aluminium based bimetal bearings.

Multi-layered components have been observed to exhibit different fatigue crack growth behaviour than those of monolithic construction. Particular attention has been given to the behaviour of a fatigue crack as it approaches a bi-material interface. Erdogan and co-workers [1,2] investigated the near tip stress and strain fields of a crack impinging normally onto an interface between two dissimilar elastic materials. This work was extended by He and Hutchinson [3] to an investigation of the factors determining whether an impinging crack would deflect along an interface or pass through it.

* Corresponding author. Tel.: +44-2380-592443; fax: +44-2380-593016
E-mail address: mrjl@soton.ac.uk (M.R. Joyce).

0921-5093/02/$ - see front matter © 2002 Published by Elsevier Science B.V.
PII: S0921-5093(02)00279-4

The behaviour of fatigue cracks approaching an interface was experimentally investigated by Suresh et al. [4,5], who considered a bi-material system comprising a ferritic and an austenitic steel, these materials having similar elastic properties and yield stress, but differing strain hardening rates and ultimate tensile strength. It was observed that a fatigue crack approaching normally to the interface from the harder side, would pass through the interface undeflected, whilst a crack approaching from the softer side showed reduced crack growth rate, crack deflection and finally arrest. It was thus demonstrated that an interface between two plastically dissimilar materials had the potential to severely affect the propagation behaviour of an approaching fatigue crack. Pippan and Flechsig [6], who tested combinations of steels with significant plastic mismatch, but almost identical elastic and thermal properties, provided further experimental evidence of this phenomenon.

The material system tested by Suresh et al. [4] was also considered by Sugimura et al. [7], who repeated much of the earlier experimental work, but also carried out a numerical investigation using the J-integral to characterise the driving force and monitor its variation for a propagating crack under quasi-static conditions. Assuming small-scale yielding around the crack tip required that only one material be modelled as elasto-plastic while the other could stay exclusively elastic. The J-integral was calculated by the finite element method (FEM) via the domain-integral formulation proposed by Li et al. [8]. In agreement with previously reported experimental results, it was found that a crack approaching the interface from the softer side experienced a considerable drop in driving force as it neared the interface; it is this shielding that causes the experimentally observed reduction in fatigue crack growth rates. Conversely when a crack embedded within the harder material was considered, anti-shielding causing increased crack growth rates was observed as the crack approached the interface.

Similar conclusions were reached by Kim et al. [9] who applied the same global approach with the two parameter J–Q theory, but also a local approach based on either brittle or ductile fracture. Kolednik [10,11] provided a theoretical argument linking the change in crack driving force as a crack approaches an interface to the yield stress gradient, developing analyses for the prediction of this effect.

The aim of this paper is to contribute to a better understanding of the fundamental fatigue behaviour of multi-layered bearing materials through the application of advanced modelling strategies such as those mentioned above. The use of J-integral as a means of characterising and assessing the driving force for fracture is extended further to the particular conditions bearing material systems are subjected to, namely large-scale plasticity and variation of elastic as well as plastic properties. Using FEM modelling, the present investigation not only assesses the degree of crack shielding or anti-shielding evolved due to the presence of material interfaces but also attempts to predict the onset and orientation of crack deflection as the crack propagates through the bearing lining towards the backing. The ultimate objective of this analysis is to explain experimentally observed fatigue behaviour in bearings and qualitatively assess the crack growth tendencies in new bearing designs.

2. Bearing material system and fatigue testing

The material system considered is typical of a modern plain bearing, comprising a lining layer of Al–Sn–Si alloy bonded to a thicker steel backing layer via a thin Al foil interlayer. The Al alloy lining material is multi-phase, with both the Si and Sn existing as distinct spheroidal and reticular secondary phases, respectively. The bearing material system was available as a flat sheet in the condition immediately prior to bearing forming. Bend bar samples ($80 \times 20 \times 2$ mm) produced from this material were used for fatigue testing, since they allowed easier and more precise crack monitoring than finished bearings. Prior to testing the surface of the lining material was highly polished both to allow surface replication and ensure consistent thickness between samples, the layer thicknesses in prepared samples are given in Table 1.

Since the purpose of the investigation was to assess the fundamental fatigue behaviour of the material system, no attempt was made to replicate the in-service loading in the laboratory; rather a simple three-point bend loading geometry with a span of 25mm, shown in Fig. 1, was adopted. The fatigue tests were carried out using an Instron 8502 servo-hydraulic fatigue testing machine. Cyclic loading with a maximum load of 500 N and a load ratio of 0.1 applied at a frequency of 10 Hz, with periodic interruptions to allow crack monitoring via surface replication. The tests were terminated according to a compliance criterion, such that mature fatigue cracks existed in the lining material, but before gross sample deformation occurred.

Fatigue cracks were seen to initiate at multiple points on the sample surface in the region of maximum bending stress. Crack initiation sites were principally associated with the interface between Si secondary phases and the surrounding matrix. Early fatigue crack growth behaviour was seen to be highly microstructurally dependent, the crack tip appearing to preferentially propagate along slip bands through the softer Sn phase and around the harder Si phase. Due to the sheer multiplicity of crack initiations, coalescence events were seen to be common and to occur throughout the test

Table 1
Layer thickness and material properties

Material	Layer thickness (mm)	Young's modulus (GPa)	Poisson's ratio	Yield stress (MPa)	Ultimate tensile stress (MPa)
Al–Sn–Si lining	0.45	69.8	0.33	56.6	172.9
Al interlayer	0.05	70	0.3	28	76
Steel backing	1.50	207	0.3	350	520

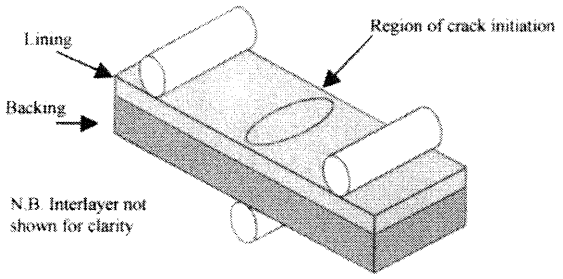

Fig. 1. Fatigue test specimen and geometry.

duration. Whilst a dominant failure crack was built up through successive coalescence events, it was observed that uncoalesced cracks showed a severe reduction in crack growth rate at a critical surface length of approximately twice the lining thickness.

In addition to the surface observations made via acetate replication, samples were also sectioned in order to investigate the sub-surface fatigue behaviour. A micrograph of a section containing a fully developed crack (Fig. 2) shows that, having initiated at the sample surface, a fatigue crack propagates towards the interface in a direction more or less normal to the sample surface. Upon approaching the interlayer, rather than continuing to propagate into the steel backing, the crack is seen to bifurcate and continue to propagate along the interlayer perpendicular to its earlier growth direction. It is thought that the observed reduction in surface crack growth rate corresponds with the change in sub-surface propagation mode. A more thorough description of the fatigue behaviour observed in this material system is given in Joyce et al. [12]. The purpose of the ensuing numerical investigation was to link this behaviour to the macroscopic properties of the layers through the fundamental concepts and principles of fracture mechanics.

3. Finite element model methodology and formulation

A series of finite element models were created using ANSYS [13], a general-purpose finite element code, to investigate the subsurface fatigue crack behaviour observed in experimental samples. The thickness and key material properties of the individual layers are given in Table 1. Experimentally obtained elasto-plastic strain hardening curves from the Al–Sn–Si lining and steel backing materials are given in Fig. 3. The same information was also provided for the aluminium foil interlayer and all elasto-plastic data were entered into ANSYS using its multi-linear isotropic hardening plasticity model. Since considerable plastic deformation was anticipated, all analyses were performed using large strain theory. As previously mentioned, unlike the assumptions by Sugimura et al. [7], the material layers considered here have differing elastic properties in addition to their plastic dissimilarity. All the models were loaded identically, in a manner simulating the arrangement of Fig. 1. Fig. 4 shows in greater detail the applied load and constraints. Plane strain conditions

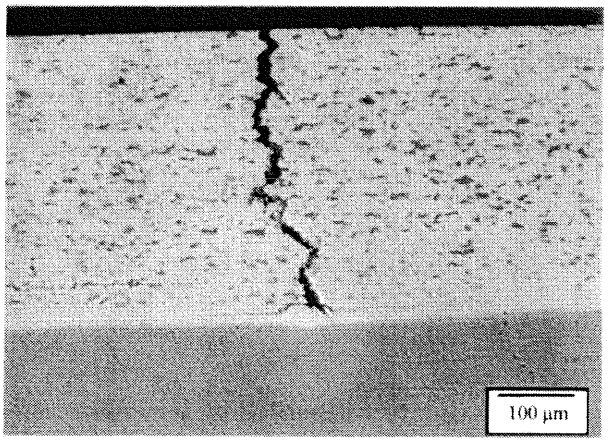

Fig. 2. Observed sub-surface crack morphology.

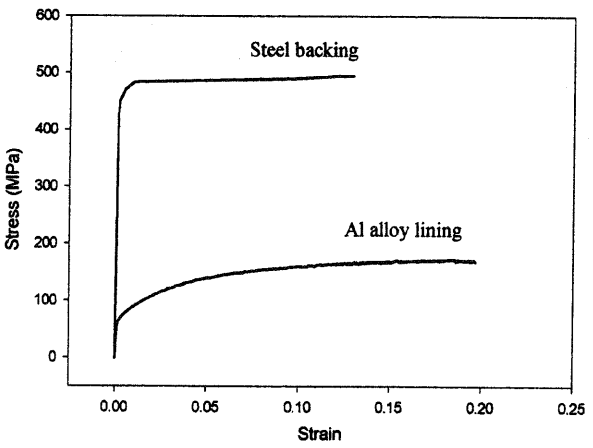

Fig. 3. Tensile stress–strain curves for lining and backing materials.

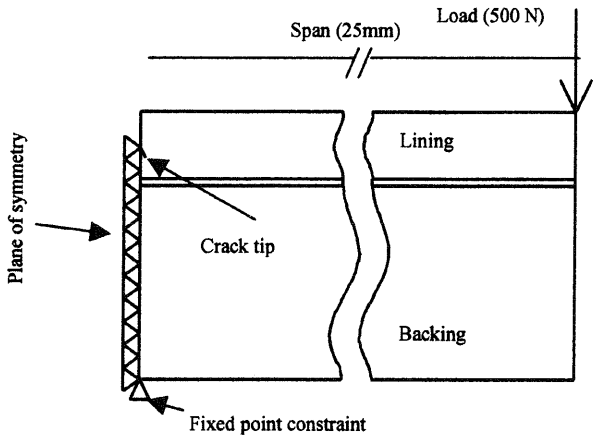

Fig. 4. Schematic view of two-dimensional solid model with loading and constraints.

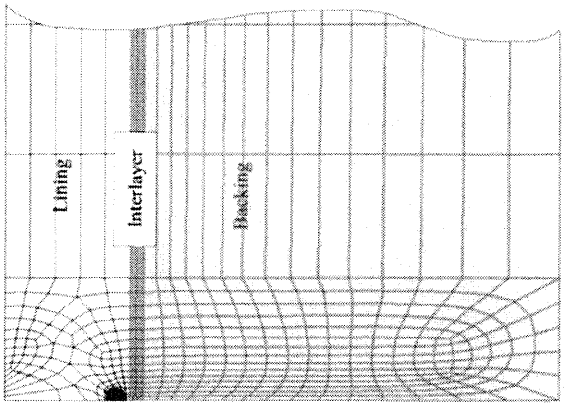

Fig. 5. Finite element model geometry.

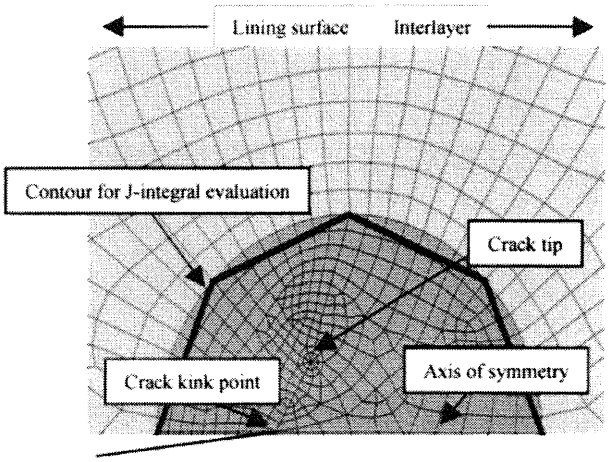

Fig. 6. Detail of finite element model around crack tip.

were adopted since the specimen width was large compared to its thickness (c.f. $W=200$ mm, $t=2$ mm). The additional material to the right of the load was not included in the model, as it is free from stress and would only add to the computational cost without providing any useful information.

For a true representation of surface cracks, a three-dimensional model would be appropriate. However, it was noted that, due to the multiple crack coalescence causing the crack depth to be small compared to its length, the crack shape could be approximated by its two-dimensional section through the centre of the sample, normal to the plane of maximum bending stress. Experimental observations of sections of a real bearing have shown that the interfaces between the layers are not smooth as modelled here, but fairly irregular. It was thought however that the omission of this feature would not compromise the integrity of the model, since the deviations from smoothness are small compared to the model dimensions. By assuming a symmetric crack tip bifurcation rather than a single deflection, the crack geometry may also be considered symmetric relative to the plane of crack growth. Thus a reduced-size, computationally efficient finite element model was developed. A mixture of free and mapped meshing with 8-node quadrilateral elements, as shown in Fig. 5, was used to control the mesh density and enhance the computational efficiency of the model. The detail of the model around the crack tip is shown in Fig. 6; it includes part of the undeflected crack of variable length, and a short fixed length ligament, which may be deflected at an arbitrary angle.

The crack was modelled at a number of discrete lengths as a means of artificially simulating crack growth through the lining. It was thus possible to assess the effect of crack tip proximity to interface on the near tip stress and strain fields. Ideally, simulation of fatigue behaviour requires the application of a cyclic loading history, which leads to the prediction of a residual plastic wake building up behind the crack tip. This closure effect was however considered beyond the purely fracture mechanics approach of the current work, therefore no effect of past loading history is accounted for in the results presented.

The applied load was static, monotonically increasing from zero to its maximum amplitude of 500 N without unloading. This resulted in a maximum tensile stress in excess of 100 MPa on the lining surface of the uncracked strip. Referring to the elasto-plastic properties of the lining displayed in Fig. 3 reveals that the central volume of the lining, within which the crack is initiated and then allowed to propagate, is fully plastic at maximum load. It was thus thought appropriate that the crack driving force be represented by the J-integral [14] given by

$$J=\int_{\Gamma} w\mathrm{d}y-\int_{\Gamma}\left(T_x\frac{\partial u_x}{\partial x}+T_y\frac{\partial u_y}{\partial x}\right)\mathrm{d}\Gamma, \tag{1}$$

where T_x, T_y are the components of traction vector, u_x,

u_y the components of displacement vector, Γ any path surrounding the crack tip and w the strain energy density.

$$w = \int_0^{\varepsilon_{ij}} \sigma_{ij}\, \mathrm{d}\varepsilon_{ij}. \tag{2}$$

The tensor notation for stress σ_{ij} and strain ε_{ij} ($i, j = 1, 2$) used in Eq. (2) implies dependence on the Cartesian co-ordinates $x_1 = x$, $x_2 = y$ and summation over repeated indices. The traction vector components T_x and T_y are determined from the stress solution according to

$$T_x = \sigma_{xx} n_x + \sigma_{xy} n_y, \tag{3a}$$

$$T_y = \sigma_{xy} n_x + \sigma_{yy} n_y, \tag{3b}$$

where $\boldsymbol{n}$ is the unit outer normal vector to path Γ.

The J-integral was evaluated along a semi octagonal contour Γ inscribed in a circle of radius 0.0125 mm surrounding the deflected ligament of length 0.005 mm, whilst the centre of the circle was kept 0.0025 mm ahead of the crack kink point, as shown in Fig. 6. It is noted that the contour always terminates on the straight crack surfaces parallel to the x-axis. Since the various bearing materials have different elasto-plastic properties, the contour is not allowed to cross a material interface. This imposes a limit on the proximity of the crack tip to an interface since sufficient space must remain ahead of the crack in order to include the semi octagonal contour. In practice this was not found a severe restriction in the case of cracks propagating solely within the lining, but did limit the number of cases analysed when the crack tip lay within the very thin interlayer.

The models were designed to enable two parameters to be investigated; the first of these was simply the crack tip driving force, the second being the preferential deflection angle. The former simply required a single undeflected crack to be 'propagated' through the material in a number of steps and, at each crack length increment, the J-integral around the crack tip to be assessed. The latter was determined from the series of deflected crack extensions, assuming that the crack would propagate in the direction which produced the highest J, that is, the highest crack tip driving force.

The analysis had, therefore, to be applied several times for different deflected angles. Typically solutions were obtained for crack deflection angles in the range from 20 to 90° in 5° increments. Re-meshing was required with a new deflection angle but the total number of elements changed only slightly from the previous step. After this cycle of computations, the length of the undeflected crack would be increased to bring the crack tip nearer the interlayer boundary and a new set of computations started with the same range of deflection angle increments. This two-stage incremental process was implemented using a series of parametric design language commands within the input ANSYS batch file allowing looping and incremental parameter value change. In this way it was possible to perform several hundred distinct analyses sequentially without requiring user input. This contributed considerably to the speed at which results could be produced.

The non-linear elasto-plastic solution was performed and stored at a number of ANSYS-defined steps. For the step size adopted, it was found that typically 50–60 iterations are required to reach convergence within each step. When the solution at the maximum load was reached, the crack tip J-integral was calculated along the semi octagonal contour shown in Fig. 6 using Eqs. (1), (2) and (3) noting that the unit normal may be mapped directly onto the path from the solution database. It was expected that the contour used in the current work would be at least partially within the crack tip plastic zone. Hence the relation between stress and strain would be non-linear and the strain energy integral (2) must therefore be calculated numerically. This was achieved by adopting the following approximation

$$w \approx \sum_q \sigma_{ij}\, \delta\varepsilon_{ij} \equiv \sum_q \left(\frac{\sigma_{ij}^q + \sigma_{ij}^{q-1}}{2}\right)(\varepsilon_{ij}^q - \varepsilon_{ij}^{q-1}), \tag{4}$$

where q is the solution sub-step number.

The second integral in the J-integral expression is more complex, but depends only on the final values of the traction and displacement vectors $\boldsymbol{T}$ and $\boldsymbol{u}$, respectively. Hence numerical step-by-step integration is not required. In order to find the derivatives of the displacement components, the path was shifted a small distance Δx equal to 1% of total path length in the positive and negative x directions. In each shifted position, the displacements u_x and u_y are mapped onto the path and the derivatives can be evaluated according to;

$$\frac{\partial u_x}{\partial x} \approx \frac{u_x^+ - u_x^-}{\Delta x}, \tag{5a}$$

$$\frac{\partial u_y}{\partial x} \approx \frac{u_y^+ - u_y^-}{\Delta x}. \tag{5b}$$

Combining these results with the values of the traction vectors found using Eq. (3), it is possible to evaluate the second integral along Γ, and then combine it with the result obtained from Eq. (4) to generate a value for the J-integral. It should be noted that since the contour is semi-octagonal and represents half of a symmetric model, the calculated value should be multiplied by a factor of two to produce the correct value of J. The accuracy of the numerical evaluation of the J-integral was tested by applying it to the three-point bend arrangement shown in Fig. 4, but with the strip having uniform elastic properties. The FEM predictions of the J-integral for various crack lengths were found almost

identical to those obtained analytically using the relevant linear elastic fracture mechanics formula for the stress intensity factor.

4. Results

4.1. Bi-layer bearing representation

Before considering tri-layer systems such as the one described earlier, it was decided to apply the developed analysis techniques on a simpler bi-layer material system. Considering the properties of the various layers given in Table 1, it is seen that the lining material and the pure aluminium used in the interlayer have very similar elastic properties. Hence, it was thought reasonable to assume that these materials could be combined together in a single layer, using common properties. Further examination will reveal subsequently the implications of these materials having very dissimilar plastic behaviour.

A graph of the J-integral value against non-deflected crack length is given in Fig. 7. The crack was forced to propagate along the direction normal to the interface in 10 μm steps from an initial length of 0.1 mm to a final length of 0.485 mm. As expected, initially the apparent crack tip driving force increased fairly linearly with crack length, before reaching a maximum value at a crack length equivalent to approximately 75% of the lining thickness. Beyond this point, the crack tip driving force was seen to drop sharply as the crack continued to propagate towards the lining-backing interface. This trend continued up to the final crack length considered. The corresponding final value of crack tip driving force was almost 50% lower than its maximum.

In order to investigate the directional propensity of the crack tip, at each increment of crack length, the crack tip deflection angle was varied from 20 to 90° in 5° increments, and the crack tip driving force evaluated. Smaller deflection angles than 20° were not considered since they would result in a very distorted mesh between the deflected ligament and the axis of symmetry. It was felt that this poor meshing would compromise the accuracy of any solutions acquired at such low deflection angles.

For each crack length the ratio of the J-integral at angle ϕ to that at angle 0° (J_ϕ/J_0) was plotted against deflection angle. This graph is shown in Fig. 8, where it can be noted that, for shorter crack lengths, maximum crack tip driving forces were recorded at smaller deflection angles. In contrast, when the crack is longer and approaching the interface, the maximum crack tip driving force was recorded at the maximum deflection angle of 90°. It is worth noting that the change from a propensity for continued straight propagation to one for deflection occurs at a similar crack length to that at which the gradient of the crack tip driving force for the bi-layer system is seen in Fig. 7 to begin to drop. However, this transition occurs at a crack length of less than 0.3 mm, which is considerably shorter than the crack length at which deflection was observed in experimental samples. This indicates that not including the discrete interlayer in the model was a critical omission.

4.2. Tri-layer bearing representation

As pointed out above, the behaviour predicted by the analysis of the bi-layer model of the bearing does not seem to be consistent with the experimental sub-surface crack behaviour depicted in Fig. 2. In order to bring the model closer to the true material system under investigation, the aluminium foil interlayer was incorporated as a separate layer with the distinct properties listed in Table 1. It was possible to grow the crack through the lining material as before, however due to the small

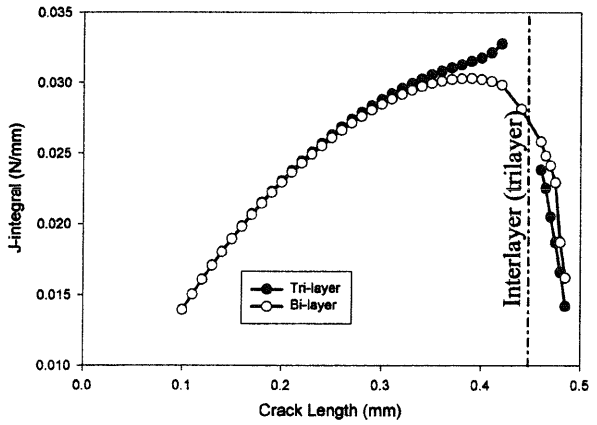

Fig. 7. Predicted J-integral variation with crack length in bi- and tri-layer models.

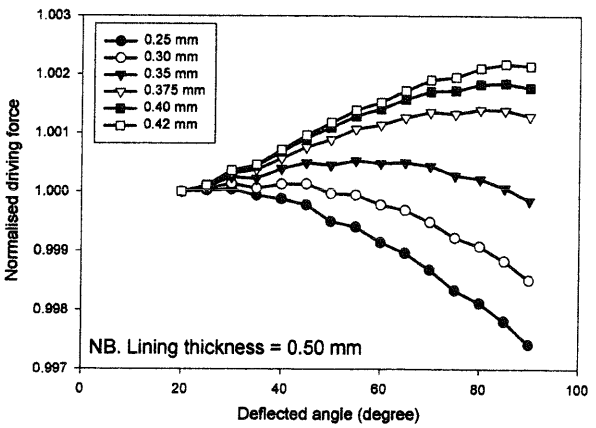

Fig. 8. Predicted J-integral dependence on crack deflection angle in bi-layer bearing model.

thickness of the interlayer compared with the size of the crack tip contour, it was not possible to obtain many results with the crack having penetrated into the interlayer.

A straight crack was grown from an initial length of 0. 1 mm (corresponding to ~22% lining thickness) to a final length of 0.42 mm (~93% lining thickness). This process brought the crack tip as close as possible to the interface between the lining and the interlayer, before the crack tip contour began to interfere with the interface. Then a second modelling run was performed with the crack tip propagating within the interlayer. Due to the limitations posed by the size of the J-integral contour, it was only possible to obtain results at crack lengths between 0.46 and 0.485 mm, which correspond to between 20 and 70% of the interlayer thickness.

The predicted variation of crack tip driving force with crack length is shown in Fig. 7 together with the respective results from the bi-linear model for comparison purposes. It was seen that as the crack grew through the lining material, the apparent crack tip driving force continued to rise, indeed showing an increased rate as the crack tip approached the interlayer, rather than dropping off as had been the case with the earlier bi-layer model. In contrast, the results within the interlayer show a steep downward trend in the crack tip driving force, indicating severe shielding with continued propagation towards the steel backing.

The results assessing crack tip directional propensity for the tri-layer case shown in Fig. 9, it can be seen that shorter cracks, growing solely within the lining material will tend to propagate straight towards the interface. However, once the crack tip penetrates into the interlayer, the limited range of predictions indicate a swift transition away from the mode I direction to a 90° deflection. These deflection results are consistent with the reduction in driving force predicted when the crack tip was forced to grow straight towards the backing.

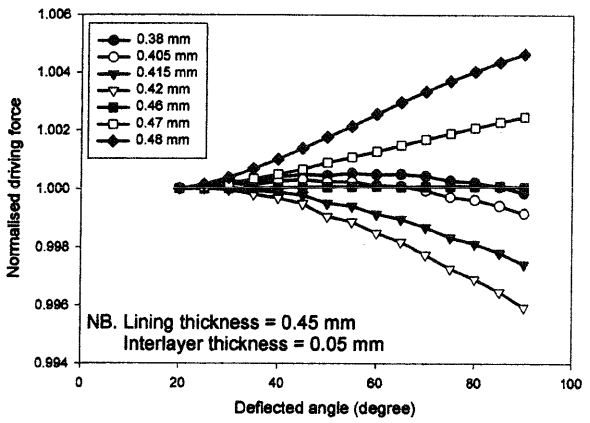

Fig. 9. Predicted J-integral dependence on crack deflection angle in tri-layer bearing model.

5. Parametric studies

A number of conceptual bearing designs were considered to study the effect of variable interlayer thickness and material properties. The aim of this parametric study was to attempt to predict the likely fatigue crack behaviour in these material systems and possibly make some assessment of fatigue life through the techniques described in the previous sections. In addition to the bi- (case 1) and tri-layer (case 2) models already analysed, six additional bearing systems (cases 3–8), shown schematically in Fig. 10, were considered. In all cases the lining and backing material had the same properties as listed in Table 1 and the backing thickness was kept constant at 1.5 mm. The other construction details of the conceptual bearings are given in Table 2.

The materials designated Int-2 and Int-3 are an Al–Si–Mg–Cu alloy and an Al–Cu–Mg–Mn alloy respectively. Whilst neither of these are a realistic replacement for pure Al in bearing interlayer applications, the variation in their plastic properties, given in Table 3, may be used to investigate any corresponding trend in predicted bearing behaviour.

5.1. Effect of interlayer plasticity

The effect of altering the material properties of the interlayer can be seen in Fig. 11 where the driving force results for the model with standard interlayer thickness (10% of the total lining thickness) but gradually increasing hardness (cases 2, 3 and 4) are plotted. The bi-layer results (case 1) are also included since this case corresponds to an interlayer having identical properties to those of the lining. In all cases, the crack tip driving force initially increases with crack length. While it continues to increase as the crack tip approaches the soft interlayer (case 2), in all other cases, it attains a maximum at a certain crack length. The drop in driving force associated with the crack tip approaching a hard

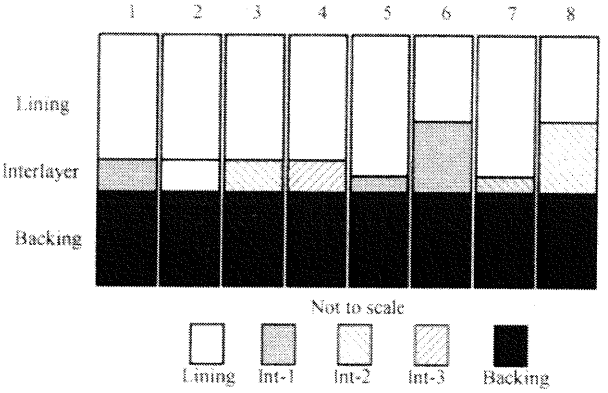

Fig. 10. Schematic diagrams of layered structures used in parametric studies.

Table 2
Conceptual bearing details for parametric studies

Bearing case	Al–Sn–Si lining thickness (mm)	Interlayer material	Interlayer thickness (mm)
1	0.5	No interlayer	N/A
2	0.45	Int-1	0.05
3	0.45	Int-2	0.05
4	0.45	Int-3	0.05
5	0.475	Int-1	0.025
6	0.25	Int-1	0.25
7	0.475	Int-2	0.025
8	0.25	Int-2	0.25

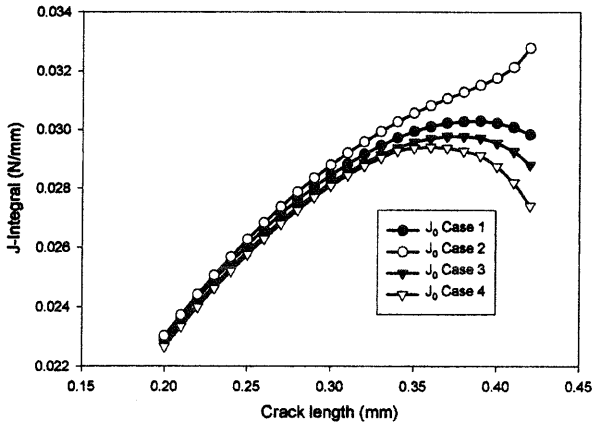

Fig. 11. Effect of interlayer plastic properties on deflectional crack behaviour.

interlayer starts earlier and becomes more pronounced with increasing interlayer hardness. J-integral computations around deflected crack tips were also performed for cases 3 and 4; the results were similar to those obtained for case 1, that is, they showed a tendency for early crack deflection. This tendency shifted to shorter crack lengths as the interlayer yield stress and amount of strain hardening were increased.

5.2. *Effect of thickness-soft interlayer*

In addition to varying the properties of the interlayer, bearing designers are also interested in the effect of its thickness relative to that of the lining material. The parametric study on the interlayer thickness effect was initially performed using Int-1, which is much softer than the lining material. Keeping the total lining thickness constant at 0.5 mm, cases 5 and 6 were generated from case 2 by, respectively, reducing the original interlayer thickness to 5% and increasing it to 50% of the total lining thickness. The crack tip driving force variations with crack length for all cases are shown in Fig. 12. Three very distinct types of behaviour can be noted. Compared with the results from case 2 within the range of crack length modelled (0.22–0.42 mm), the previously observed crack tip anti-shielding was not observed in case 5, rather a very slight decrease in crack tip driving force coupled with a propensity for deflection was predicted as the crack reached its maximum length. In case 6, the results show that a short crack existing in the lining only appears to have a much higher driving force than a similar crack in a standard bearing system. Once the crack was allowed to propagate into the interlayer however, the driving force dropped off markedly and a propensity for deflection became evident almost immediately. The crack shielding or anti-shielding trends shown in Fig. 12 were confirmed by corresponding crack driving force calculations from deflected crack tips, such as those shown in Figs. 7 and 8.

5.3. *Effect of thickness-hard interlayer*

The reference geometry for this parametric study is that of case 3 from which cases 7 and 8 are generated as in the previous study by the same changes of the reference thickness. The relevant data from Tables 1 and 3 indicate that the adopted interlayer (Int-2) has a considerably higher yield stress but also a lower strain hardening rate than the lining. The plots of results in Fig. 13 indicate similar trends in J-integral variation for

Table 3
Interlayer properties

Material	Young's modulus (GPa)	Poisson's ratio	Yield stress (MPa)	UTS (MPa)	Elongation at UTS (%)
Int-1 (~ pure Al)	70	0.3	28	76	39
Int-2 (Al–Si–Mg–Cu)	70	0.3	74	152	21
Int-3 (Al–Cu–Mg–Mn)	70	0.3	97	186	18

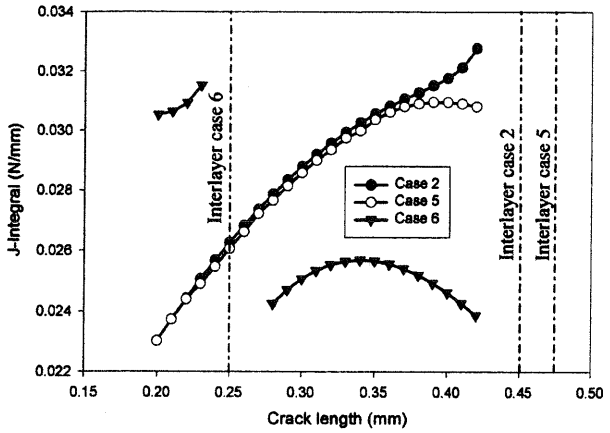

Fig. 12. Effect of interlayer thickness on deflectional crack behaviour—soft interlayer.

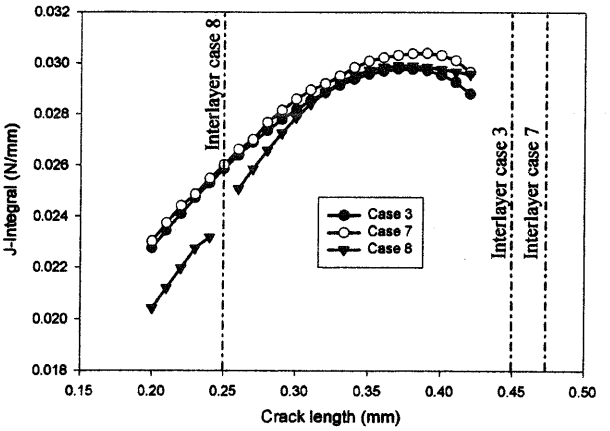

Fig. 13. Effect of interlayer thickness on deflectional crack behaviour—hard interlayer.

all cases. It is worth noting that shielding is slightly delayed with the thinner interlayer, while the crack driving force is lower within the lining and shielding is not much affected with the thicker interlayer. These trends are opposite to those observed when the thickness of the soft (~ pure Al) interlayer was varied in thickness. Again, the investigation on propensity for crack deflection produced results consistent with the above observations.

6. Discussion

6.1. Implication and validity of selected methodology

The assumption of monotonic loading history allowed the adoption of an essentially fracture mechanics approach with the near tip J-integral evaluated at maximum load. Under such conditions, the J-integral is a valid indicator of crack tip driving force intensity

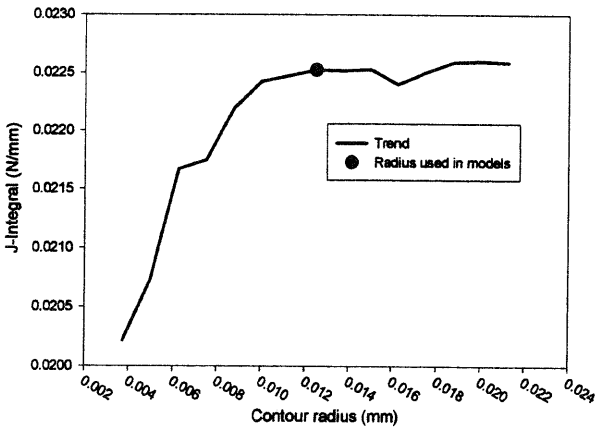

Fig. 14. Path dependence of J-integral.

[14]. Its path-independence under elasto-plastic deformation was confirmed numerically, provided the path radius was above a certain minimum, which depended on the size of the tip elements, as shown in Fig. 14. A near tip integration contour had to be used since a far field contour would have to cross material interfaces and thus invalidate the requirement for homogeneity. Thus, in contrast to Sugimura et al.'s work [7], it was not possible to correlate the near-tip plastic with any far-field elastic behaviour. On the other hand, it was demonstrated how the J-integral methodology for assessing fatigue crack growth could be applied to a realistic system rather than an idealised one and still predict the trends noted in earlier investigations [4–7].

It should be noted that the J-integral path around a deflected tip still begins from and ends at the surfaces of the main, undeflected crack, the integral itself is therefore path-independent but continues to represent the crack driving force for the crack propagating in the direction normal to the interface. Along the kink at the end of the main crack, a mixed mode I–mode II fracture develops and the respective stress intensity factors can be expressed in terms of that for the main crack if linear elastic fracture mechanics could be applied [15]. It should however be clear that the J-integral plots shown in Figs. 8 and 9 indicate the effect of the deflection angle on the crack driving force of the main crack assuming that the shape of its tip remains the same as it propagates towards the interface [14].

6.2. Standard bearing system

Initially, J-integral calculations were performed on a bi-layer model of the standard bearing tested at Southampton. The validity of several of the adopted techniques was first assessed through this simpler system. The plot in Fig. 7 shows that, for small crack lengths, it is more favourable for the straight crack to continue propagating towards the single material interface. How-

ever, as the crack approaches the interface, the plastic zone developing in the lining cannot penetrate into the steel due to the lining being much softer than the steel backing; indeed the steel remains entirely elastic during the analysis. Thus the shape of the plastic zone ahead of the crack tip becomes highly distorted causing the predicted rapid increase in extrinsic shielding. This is combined with a marked tendency for the crack to deflect or bifurcate.

As Fig. 8 shows, the transition from a propensity for continued straight propagation, to one for 90° deflection begins at a crack length of around 0.3 mm (60% of the lining thickness) and evolves over a crack extension of around 0.1 mm (20% of the lining thickness). This indicates a gradual increase in shielding with increasing crack length, which should, in reality, correspond to a gradual bifurcation towards the crack tip. This type of behaviour has indeed been observed in early bearing designs comprising a steel backing and an Al–Si lining material without soft bonding interlayer [16], as well as in a recent experimental study [6]. It is however considerably different from the experimental observations on the standard bearing tested at Southampton, which includes a thin and soft interlayer (compared to the rest of the lining).

As shown in Fig. 7, the analysis of the respective trilayer model predicted that, the apparent crack tip driving force increased at a higher rate as the crack approached the interlayer from the lining side, in contrast to the previously observed reduction in the bilayer case. This is apparently due to the close proximity of the soft interlayer, which increases the local compliance near the crack tip (similar to a free surface condition) causing an increase in crack tip plastic zone size (which extends through the interlayer). The anti-shielding predicted by the model when a crack approaches an interface from the less compliant side, has been confirmed experimentally [7]. It is also consistent with the results of Fig. 9, which show no propensity for deflection away from the mode I crack opening direction for cracks short of interlayer penetration. This trend is reversed when the crack is allowed to penetrate into the interlayer. Although it was not possible to model very small changes in penetration due to meshing constraints, it is clear from Fig. 7 that the J-integral drops markedly with further propagation towards the backing. Essentially, the interlayer/backing system now behaves as a bilayer bearing with a very thin lining, where the plastic zone formed in the very soft interlayer is highly contained by the proximity of the elastic backing, causing shielding. As was observed earlier, these high levels of extrinsic crack tip shielding are associated with a propensity for deflection. As shown in Fig. 9, the change from 0 to 90° is very sharp (it is noted over a crack extension of 0.01 mm), conforming to the experimental evidence of Fig. 2.

6.3. Role of interlayer material properties

Interlayer yield stress and strain hardening behaviour were investigated as potentially critical parameters in determining the point at which crack deflection occurs. It is seen in Fig. 11 that a bearing containing an interlayer softer than the lining, would exhibit crack anti-shielding as the crack tip approaches the interlayer, and that crack deflection would occur only after interlayer penetration. Increasing the strength of the interlayer to that of the lining is seen to remove the crack anti-shielding. Further increases in interlayer strength are seen to promote increased shielding and early crack deflection.

These effects can be explained by the changing nature of compliance mismatch between the lining and the interlayer. In the case of a soft interlayer, the approaching crack encounters an area of increased compliance, which causes the plastic zone size to expand and hence the crack tip driving force to increase. When the interlayer is made harder than the lining the reverse is true, the plastic zone of the approaching crack is constrained by the reduced compliance from the hard interlayer, hence causing shielding and crack deflection. It therefore appears that the inclusion of an interlayer material having a yield stress considerably lower than that of the lining material may be detrimental to the overall fatigue performance of the bearing.

6.4. Layer geometry effects

Another bearing design feature investigated was interlayer thickness. The ratio of lining to interlayer thickness was allowed to vary, however their combined thickness was kept constant. The effect of changing the thickness of a soft interlayer was first investigated. Fig. 12 shows that, reducing the thickness removes the previously observed anti-shielding as the crack approaches the interlayer. This is attributed to the thinner soft interlayer no longer being able to buffer the approaching crack from the shielding effects of the very stiff steel backing. Hence local compliance just prior to interlayer penetration will be higher in this case than in the standard bearing, leading to some degree of shielding being developed. When the interlayer thickness was increased to half the overall lining thickness, initially greatly enhanced crack driving force was observed. However, once the crack had penetrated the interlayer, the very low compliance of the steel caused high levels of shielding to be evolved quickly.

The effect of changing the thickness of an interlayer stronger than the lining can be seen in Fig. 13. These results suggest that a bearing containing a reduced thickness interlayer exhibits slightly less shielding at a given crack length than that with the reference thickness. This can be attributed to the thinner interlayer

producing a smaller region of raised local stiffness within the lining adjacent to the interlayer. It is hard to assess the overall effect of increased interlayer thickness on crack growth, since the crack tip driving force is initially low due to the high local compliance of the lining relative to that of the thick interlayer, but rises quickly after interlayer penetration. However, it also appears that a small amount of enhanced shielding in evident as the crack approaches the interlayer. Linking this to the observed experimental behaviour, it is likely that such an early reduction in sub-surface crack tip driving force will also result in a premature reduction in surface crack growth rate. Therefore, this particular bearing design may potentially offer enhanced resistance to fatigue crack growth.

7. Summary and conclusions

It has been proposed that, for cracks propagating through multi-layered materials [4], the local compliance ahead of the crack is reduced in the case of a crack approaching the interface from the softer side, and raised when the crack approaches from the harder side. It has also been argued that a drop in local compliance precludes continued crack propagation in the nominal mode I direction, hence the crack deflects.

Finite element models have confirmed this proposition in the case of modern automotive plain bearing designs. It was shown that their layered material structure exerts a considerable influence on the mesoscopic growth of fatigue cracks. In the case of a standard bearing with aluminium lining, a fatigue crack entering the Al bonding interlayer was shown to undergo a sharp increase in near tip shielding, associated with a propensity for crack deflection, which correlates well with experimental observation. Further to earlier numerical work [7], the present study also included a fracture mechanics interpretation of the marked change of behaviour from a nominally mode I direction to a 90° deflection or bifurcation.

The role of the interlayer in fatigue crack propagation has been assessed. It was found that increasing the interlayer hardness promoted increased shielding and consequently a propensity for early crack deflection. It is postulated that the magnitude of the evolved shielding is proportional to the hardness ratio of the two materials. The role of interlayer thickness was also quantified, showing that in the case of a soft interlayer, a reduction in thickness promoted enhanced shielding. Conversely, when considering hard interlayers, increasing thickness to a maximum was predicted to be beneficial. This later effect is given credence by the sponsoring companies experience with bearings comprised of a thin layer of Al–Sn coating on a thicker layer of stronger bronze, which are known to exhibit excellent fatigue properties. Therefore, it is hypothesised that a bearing with a hard thick interlayer offers potentially enhanced fatigue performance over one with a thin soft interlayer.

It would be interesting to correlate the computed changes in crack driving force as the crack propagates across interfaces of materials with different properties with Kolednik's theoretical predictions [11]. This however would require the numerical evaluation of a far-field J-integral as well as an elastic modulus gradient term since the bearing system considered in this paper consists of materials with different elastic as well as plastic properties. It was felt that the additional computations involved were beyond the scope of the present work, but such a comparison would be a valuable validating tool in further developments of the proposed methodology.

Future modelling refinements should be attempted in order to confirm the validity of the trends predicted by the adopted simplified approach but also expand the scope of the presented analysis. For instance, the analysis of the real, three-dimensional crack shape would allow the investigation of the driving force variation along the crack front. The application of cyclic fatigue loading would result in residual plastic deformation and this will undoubtedly cause closure effects, which would be enhanced when the crack deflects. A valid method to assess crack growth under cyclic loading and highly plastic conditions would be through the evaluation of the crack tip opening displacement (CTOD) [17]. This parameter in conjunction with the crack tip sliding displacement (CTSD) may be used to fully characterise the behaviour of the crack tip during both loading and unloading steps, thus accounting for the effect of accumulated plastic damage [18].

Acknowledgements

The authors would like to thank Dana Glacier Vandervell and the Engineering and Physical Sciences Research Council for financial and material support throughout the duration of this project.

References

[1] T.S. Cook, F. Erdogan, Int. J. Eng. Sci. 10 (1972) 677.
[2] F. Erdogan, V. Biricikoglu, Int. J. Eng. Sci. 11 (1973) 745.
[3] M. He, J.W. Hutchinson, Int. J. Solids Struct. 25 (1989) 1053.
[4] S. Suresh, Y. Sugimura, E.K. Tschegg, Scr. Metall. 27 (1992) 1189.
[5] S. Suresh, Y. Sugimura, T. Ogawa, Scr. Metall. 29 (1993) 237.
[6] R. Pippan, K. Flechsig, Mater. Sci. Eng. A283 (2000) 225.
[7] Y. Sugimura, P.G. Lim, C.F. Shih, S. Suresh, Acta Metall. 43 (1995) 1157.
[8] F.Z. Li, F. Shih, A. Needleman, Eng. Fract. Mech. 21 (1985) 405.
[9] A. Kim, J. Benson, A. Pineau, Int. J. Solids Struct. 36 (1999) 1845.

[10] O. Kolednik, in: Proc. ETCE 2000 & OMAE 2000: Energy for the New Millennium, New Orleans, 2000, 1047.
[11] O. Kolednik, Local variations in yield stress – A means for the design of more fracture resistant materials. Proceedings of ETCE 200 & OMAE 200: Energy for the New Millennium, February 14–17, 2000, New Orleans. ASME, Farfield, NJ.
[12] M. Joyce, S. Syngellakis, P.A.S. Reed, Mater. Sci. Forum. 331 (II) (2000) 1445.
[13] ANSYS 5.6, SAS IP, Inc., Canonsburg, PA, 1999.
[14] J.R. Rice, Proc. ASME., J. Appl. Mech. 35 (1968) 379.
[15] S. Suresh, Fatigue of Materials, Cambridge University Press, Cambridge, 1998, 307.
[16] P. Shenton, C. Perrin, Private communication, Dana Glacier Vandervell, Cawston, 1998.
[17] R. Pippan, F. Riemelmoser, K. Flechsig, in: A. Carpinteri, C.A. Brebbia (Eds.), Damage and Fracture mechanics–Computer Aided Assessment and Control, Computational Mechanics Publications, Ashurst, UK, 1998, p. 175.
[18] C. Li, Fat. Fract. Eng. Mater. Struct. 12 (1989) 59.